ASME Journal of Engineering and Science in Medical Diagnostics and Therapy
Online journal at:
https://asmedigitalcollection.asme.org/medicaldiagnostics

Effects of Combined Fatigue and Asymmetric Loading on Knee Kinematics During Walking Gait

Dumitru I. Caruntu[1]
Fellow ASME
Mechanical Engineering Department,
University of Texas Rio Grande Valley,
Edinburg, TX 78539
e-mail: dumitru.caruntu@utrgv.edu

Alfirio Trejo
Mechanical Engineering Department,
University of Texas Rio Grande Valley,
Edinburg, TX 78539

Fatigue and asymmetrical loading can alter gait mechanics, yet their combined effects on knee kinematics during walking remain under-investigated. This single-subject pilot examined how squat-induced fatigue interacts with one-hand load carriage to influence knee flexion, abduction, and internal rotation. Three-dimensional kinematics were collected using a Vicon system, and clinical knee angles were computed with a modified Grood–Suntay joint coordinate system (JCS). The protocol included normal walking (NW), asymmetrical load carriage (farmer's carry, left hand), and postfatigue trials following 25, 50, 75, and 100 body-weight squats. Fatigue was associated with increased flexion variability and greater flexion at heel strike and early stance. Abduction and internal rotation waveforms remained generally consistent across fatigue levels; however, frontal-plane variability was greatest during asymmetrical loading prior to fatigue. Stride-length variability increased markedly in the 100-squat condition, suggesting a faster but less stable gait strategy under maximal fatigue. Together, the results demonstrate joint-specific and phase-dependent adaptations to fatigue and asymmetrical loading. Increased variability, particularly in flexion, likely reflects compensatory mechanisms that redistribute mechanical demand across the lower limb. While preliminary, these findings motivate larger, bilateral studies incorporating kinetics and electromyography (EMG) to refine rehabilitation and ergonomic recommendations for loaded walking. [DOI: 10.1115/1.4070655]

Keywords: gait analysis, knee kinematics, fatigue, asymmetrical loading, motion capture, farmer's carry, squat-induced fatigue

1 Introduction

Human gait is a complex biomechanical process involving coordinated joint movement, muscle activation, and balance control. External factors such as fatigue and asymmetrical loading can alter gait mechanics and introduce compensatory strategies. These adaptations affect joint alignment, movement efficiency, and overall stability.

Asymmetrical loading, such as carrying a backpack on one shoulder, produces clear frontal-plane knee alterations, greater valgus on the loaded limb, and compensatory varus and hip abduction on the unloaded limb, demonstrating that even everyday asymmetry disrupts lower-limb alignment [1]. Independent of asymmetrical loading, increasing external load during walking produces significant six-degrees-of-freedom knee kinematic alterations, including greater knee flexion, internal tibial rotation, and lateral tibial translation [2]. Together, these findings indicate that both the distribution and magnitude of external load can meaningfully perturb knee biomechanics during gait.

Another contributing factor is fatigue, which influences gait by altering joint range of motion, muscle activation patterns, and spatiotemporal parameters. During high-intensity athletic maneuvers (e.g., unanticipated cutting), fatigue tends to reduce knee flexion at initial contact, consistent with a stiffer landing strategy [3]. However, findings in walking are mixed. Some studies report increased flexion at heel strike with fatigue [4], others report reduced sagittal-plane knee range of motion [5], no change in heel-strike flexion [6], or small, nonsignificant early-stance flexion reductions during whole-body walking fatigue [7]. Notably, even when flexion angles remain unchanged, frontal- and transverse-plane knee angles and moments can still be altered under quadriceps fatigue [6]. Fatigue can also increase step-width variability during walking, even when speed is controlled; mean step width may rise after localized fatigue and continue to increase or even trend lower after whole-body fatigue [7]. Following isolated ankle plantarflexor fatigue during normal walking (NW), participants exhibit slightly greater knee flexion during loading and reduced peak ankle plantarflexion at toe-off, with minimal contralateral changes, indicating that distal fatigue can produce modest sagittal-plane adjustments without widespread alterations in gait mechanics [8].

While the individual effects of fatigue and asymmetrical loading on gait have been studied, their combined influence remains under-investigated. This study investigates how progressive fatigue, induced through repeated squatting, interacts with asymmetrical loading to affect knee kinematics during walking. Specifically, it quantifies changes in knee flexion, abduction, internal rotation, stride time, and stride length across fatigue conditions to better

[1]Corresponding author.

Contributed by the Materials Division of ASME for publication in the Journal of Engineering and Science in Medical Diagnostics and Therapy. Manuscript received October 3, 2025; final manuscript received December 8, 2025; published online January 19, 2026. Assoc. Editor: Samson Adejokun.

Fig. 1 Vicon camera (left), laboratory (right): Overview of the laboratory and camera arrangement used to record overground walking at 100 Hz. A single subject performed normal walking and asymmetrical load carriage (farmer's carry) trials, including postfatigue conditions following sets of body-weight squats. Marker trajectories were used to compute knee clinical angles via a modified Grood–Suntay joint coordinate system.

understand compensatory gait adaptations. These findings have implications for injury prevention, rehabilitation progression, and ergonomic design in occupations involving asymmetrical loading.

2 Methodology

2.1 Experimental Setup. Motion capture data were collected using a Vicon motion capture system, Fig. 1, equipped with infrared cameras operating at a sampling rate of 100 Hz. The system was calibrated prior to each session to ensure accuracy in marker tracking. Reflective markers, Fig. 2, were placed on key anatomical landmarks. The protocol for data acquisition is detailed afterwards.

2.2 Joint Coordinate System Construction. The joint coordinate system (JCS), established by Grood and Suntay [9], was used to define the rotational movements of the knee joint. This system uses three mutually orthogonal axes: two body-fixed axes and one floating axis. The femoral coordinate system was defined by three body-fixed axes with the unit vectors: **I** (medial–lateral axis), **J** (posterior–anterior axis), and **K** (distal–proximal axis), Fig. 3. Similarly, the unit vectors of the tibial coordinate system were defined by **i** (medial–lateral axis), **j** (posterior–anterior axis), and **k** (distal–proximal axis). The joint coordinate system unit vectors are $\mathbf{e_1}$, $\mathbf{e_2}$, and $\mathbf{e_3}$. The $\mathbf{e_1}$ unit vector is the unit vector **I** of the femur's medial–lateral axis to measure flexion–extension (α). The unit vector $\mathbf{e_3}$ is the unit vector **k** of tibia's distal–proximal axis to measure internal–external rotation (γ). The floating axis, $\mathbf{e_2}$, was orthogonal to both $\mathbf{e_1}$ and $\mathbf{e_3}$ and served as the reference for abduction–adduction (β).

To construct the JCS using marker-based motion tracking, reflective markers were positioned on the femur and tibia, Fig. 2. This marker tracking setup was derived from previous studies done in the same laboratory [10,11]. The femoral medial–lateral axis unit vector **I** was defined by the vector from the medial knee epicondyle

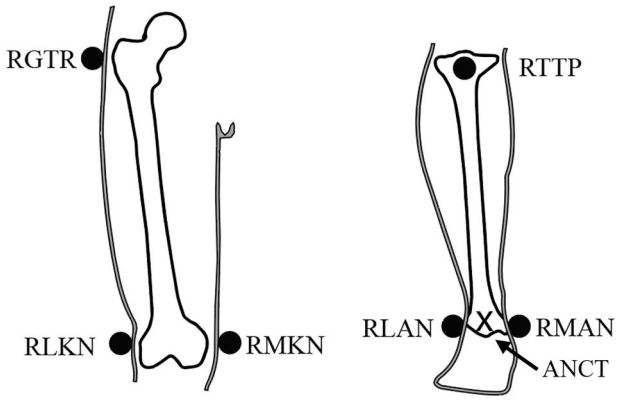

Fig. 2 Landmark and marker locations: Reflective markers placed on key landmarks used to construct the femoral and tibial segment axes: greater trochanter (RGTR), lateral/medial knee epicondyles (RLKN/RMKN), tibial tuberosity (RTTP), and lateral/medial malleoli (RLAN/RMAN). These markers define femoral axes I, J, K and tibial axes i, j, k, from which knee clinical angles are derived.

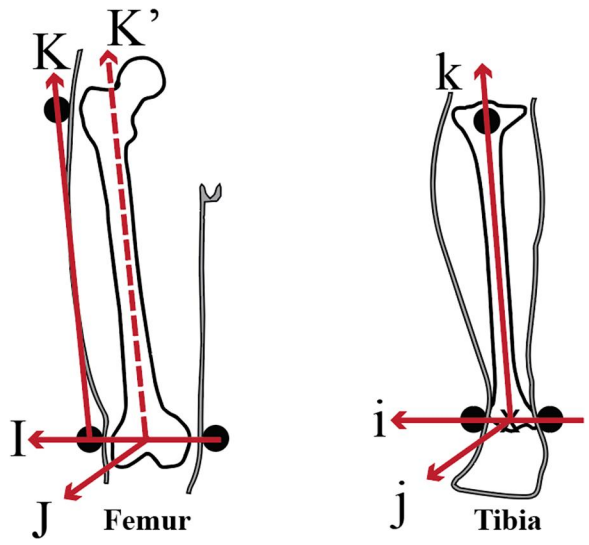

Fig. 3 Femur and tibia coordinate system: Schematic of the femoral unit vectors (I, J, K) and tibial unit vectors (i, j, k). K′ is parallel to K illustrating the femoral longitudinal axis. Clinical rotations are reported as: flexion–extension about the femoral medial–lateral axis (I), abduction–adduction about the floating axis (e_2), and internal–external tibial rotation about the tibial longitudinal axis (k). Sign conventions used throughout: positive = abduction and internal rotation.

(RMKN) to the lateral knee epicondyle (RLKN). The femoral distal–proximal axis unit vector **K** was determined from the lateral knee epicondyle (RLKN) to the greater trochanter (RGTR). The posterior–anterior axis unit vector **J** was obtained by computing the cross product of the medial–lateral unit vector **I** and distal–proximal unit vector **K** axes

$$\mathbf{I} = \frac{\mathbf{RLKN} - \mathbf{RMKN}}{\|\mathbf{RLKN} - \mathbf{RMKN}\|} \tag{1}$$

$$\mathbf{K} = \frac{\mathbf{RGTR} - \mathbf{RLKN}}{\|\mathbf{RGTR} - \mathbf{RLKN}\|} \tag{2}$$

$$\mathbf{J} = \frac{\mathbf{K} \times \mathbf{I}}{\|\mathbf{K} \times \mathbf{I}\|} \tag{3}$$

where **RMKN**, **RLKN**, and **RGTR** are the position vectors of the markers with respect to the global (laboratory) coordinate system.

For the tibial coordinate system, the unit vector **i** of the medial–lateral axis was defined by the vector between the medial ankle marker (RMAN) and lateral ankle marker (RLAN). The unit vector **k** of the distal–proximal axis was determined by the vector from the ankle midpoint (ANCT) to the tibial tuberosity (RTTP). The posterior–anterior axis (**j**) was computed using

$$\mathbf{ANCT} = 0.5 * (\mathbf{RLAN} + \mathbf{RMAN}) \tag{4}$$

$$\mathbf{i} = \frac{\mathbf{RLAN} - \mathbf{RMAN}}{\|\mathbf{RLAN} - \mathbf{RMAN}\|} \tag{5}$$

$$\mathbf{k} = \frac{\mathbf{RTTP} - \mathbf{ANCT}}{\|\mathbf{RTTP} - \mathbf{ANCT}\|} \tag{6}$$

$$\mathbf{j} = \frac{\mathbf{k} \times \mathbf{i}}{\|\mathbf{k} \times \mathbf{i}\|} \tag{7}$$

where **ANCT**, **RMAN**, **RLAN**, and **RTTP** are position vectors with respect to the global coordinate system of their respective markers. The unit vector $\mathbf{e_2}$ of the floating axis was derived from the cross product of the tibial and femoral axes

$$\mathbf{e}_2 = \frac{\mathbf{k} \times \mathbf{I}}{\|\mathbf{k} \times \mathbf{I}\|} \tag{8}$$

2.3 Clinical Angle Determination. Clinical angles were computed using the modified Grood and Suntay method. Knee flexion angle α was calculated using the approach described by Dabirrahmani et al. [12] to address limitations in the conventional method

$$\text{Flexion} = \text{atan2}\left(\frac{n|\mathbf{J} \times \mathbf{e}_2|}{\mathbf{J} \cdot \mathbf{e}_2}\right) \tag{9}$$

where

$$n = (\mathbf{J} \times \mathbf{e}_2) \cdot \mathbf{I} \tag{10}$$

For abduction and internal rotation, the conventional equations were modified to ensure consistent positive and negative angle conventions

$$\text{Abduction} = \cos^{-1}(\mathbf{I} \cdot \mathbf{k}) - 90 \text{ deg} = -\sin^{-1}(\mathbf{I} \cdot \mathbf{k}) \tag{11}$$

$$\text{Internal} = \sin^{-1}(\mathbf{e}_2 \cdot \mathbf{i}) \tag{12}$$

These calculations ensured that positive values corresponded to abduction and internal rotation, while negative values represented adduction and external rotation, maintaining clinical relevance.

2.4 Experimental Protocol. The subject performed (i) normal walking, (ii) asymmetrical load carriage (farmer's carry) with a 30-lb (13.6 kg) kettlebell in the left hand, Fig. 4, and (iii) a squat-fatigue protocol consisting of four sets of 25 body-weight squats, with a left hand farmer's-carry walking trial immediately after each set. All walking trials were conducted on an overground surface at the subject's preferred speed.

Squatting was selected to preferentially fatigue the quadriceps, the primary knee extensors during gait. Prior biomechanical modeling of the tibiofemoral and patellofemoral joints shows that the magnitude and line of action of quadriceps force substantially influence tibiofemoral kinematics and patellar tracking during weight-bearing/deep-flexion tasks [13,14]. The subject descended to at least 90 deg knee flexion on each repetition and returned to full standing; no rest was provided between sets to standardize fatigue accumulation.

2.5 Data Analysis. Raw motion capture data were exported from Vicon NEXUS into an Excel format for further processing in MATLAB. The postprocessing workflow consisted of multiple sequential steps to filter, organize, segment, and analyze gait kinematics.

First, the data were imported into MATLAB. A low-pass Butterworth filter was applied to remove high-frequency noise from marker trajectories. The filtered data were then used to create the JCS.

The JCS was constructed by defining the femoral (**I**, **J**, **K**) and tibial (**i**, **j**, **k**) unit vectors of the coordinate axes, following the modified Grood and Suntay method. The unit vector $\mathbf{e_2}$ of the floating axis was computed as the cross-product of the tibial and femoral axes. Clinical angles, including flexion, abduction, and internal rotation, were derived, ensuring alignment with clinical conventions.

To analyze gait events, heel strikes were detected based on heel z-coordinate minima. Using these heel strikes, the data were segmented into gait cycles, and each cycle was normalized to a common percentage scale (0–100%) for direct comparison across trials. An interpolation function was applied to resample the clinical angles at uniform increments of 0.1% of the gait cycle.

For each interpolated cycle, mean and standard deviation were computed at every percentage point to assess variability. Stride parameters were then calculated, including stride length, measured as the Euclidean distance between consecutive heel strikes, and step time, derived from the temporal difference between consecutive heel strikes.

3 Results

This pilot study analyzed six walking conditions: (1) NW, (2) left hand farmer's carry without squats (FC), and (3) postfatigue left hand farmer's carry trials after 25 (FC-25), (4) 50 (FC-50), (5) 75 (FC-75), and (6) 100 (FC-100) squats. Kinematic data were collected with motion capture, and joint variability was assessed for right-knee flexion, abduction, and internal rotation. The subject was a 17-year-old male (height: 5 ft 6 in/1.68 m; weight: 117 lb/53.1 kg). Self-reported fatigue ratings (0–10 scale) were 2, 4, 8, and 10 following 25, 50, 75, and 100 squats, respectively.

Across conditions, clinical-angle waveforms exhibited phase-dependent changes and nonlinear trends in variability. Variability peaked after 25 squats (FC-25), decreased during midfatigue (FC-50, FC-75), and rose slightly again at FC-100.

3.1 Flexion. Knee flexion, Fig. 5, followed a five-event signature across the gait cycle: (1) the initial contact angle at heel strike (0%); (2) the shock absorption peak during early stance (≈8–14% in this dataset); (3) the midstance valley as the limb extends under body weight (≈30–40%); (4) the terminal swing peak (maximum flexion during swing; ≈60–75%); and (5) the precontact valley, the minimum flexion just before the next heel strike

Fig. 4 Subject and single hand farmer's carry: The subject carries a 30 lb (13.6 kg) kettlebell in the left hand while walking overground at a preferred speed to induce asymmetrical loading. This condition was performed alone (FC) and repeatedly after each squat set (FC-25, FC-50, FC-75, and FC-100) to examine the interaction between fatigue and asymmetry.

(≈92–96%). These events define sagittal-plane behavior and were used as key indicators of fatigue-related change.

Under NW, baseline flexion magnitudes were modest: the initial contact angle was just under 10 deg, the shock-absorption peak was ∼15 deg, the midstance valley was ∼10 deg, the terminal swing peak was just under 60 deg, and the precontact valley was ∼5 deg. These values serve as the reference pattern against which loaded and fatigued conditions were compared.

The flexion angle at heel strike ranged from 4.43 deg (FC-50) to 25.32 deg (FC-100). The farmer's-carry baseline (FC) recorded 11.05 deg, while all squat trials except FC-100 remained below 8 deg.

The shock absorption peak increased with fatigue, from 16.25 deg (FC-25) to 34.13 deg (FC-100). Peak timing clustered in early stance, occurring earlier in FC (8.28%) and FC-100 (8.77%), and later in FC-50 (13.33%) and FC-75 (13.58%).

Flexion then decreased during the midstance valley, ranging from 5.02 deg (FC-50) to 9.33 deg (FC). All fatigue trials showed lower midstance values than FC, with FC-50 reaching a slightly deeper valley (5.96 deg) than the other squat trials.

The terminal swing peak magnitude remained relatively stable across trials, with values between 59.21 deg (FC) and 63.86 deg (FC-75). The timing of this peak was later in all squat trials compared with FC.

Finally, flexion decreased to the precontact valley just prior to heel strike. All conditions except FC-100 showed low terminal values between 4.45 deg and 5.28 deg, whereas FC-100 reached 10.98 deg, the highest precontact angle observed.

3.2 Abduction. Across all conditions, the abduction waveform pattern was consistent, Fig. 6. (Positive values denote abduction.) At initial contact (0% gait), angles were near neutral. After heel strike, the abduction decreased slightly forming a wide valley that fell near –2.5 deg at 45%. The abduction rose to ∼6 deg around terminal swing peak (60%) before returning to initial values at the next heel strike.

Under NW, abduction remained near neutral (∼0 deg) throughout stance and, similar to the other conditions, rose to ∼5 deg during late/terminal swing before returning toward 0 deg at the next heel strike.

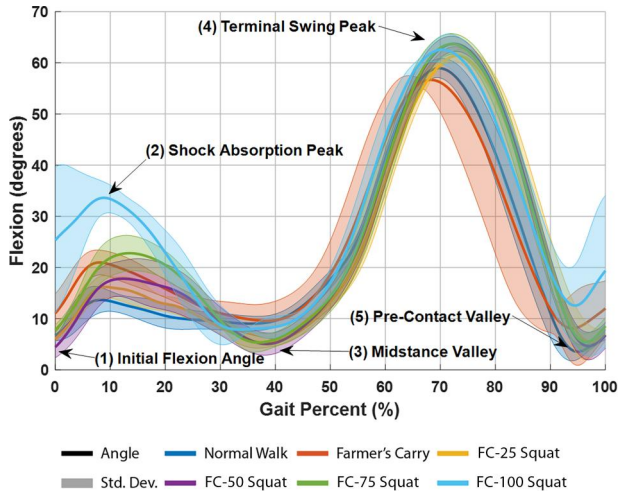

Fig. 5 Flexion angle mean and standard deviation versus percent gait: Mean (solid line) and ±1 SD (shaded area) of knee flexion angle versus normalized gait percentage (0–100%, heel-strike to heel-strike) for six conditions: NW, FC, and FC-25/50/75/100 (postfatigue). A five-event signature is evident: initial-contact angle, shock absorption peak, midstance valley, swing peak, and precontact valley. With increasing fatigue, early-stance flexion peaks increased (e.g., ∼16.3 deg at FC-25 to ∼34.1 deg at FC-100), midstance valleys deepened relative to FC, and precontact extension was incomplete at FC-100 (terminal-swing flexion ∼11 deg versus ∼4–5 deg in other trials), indicating altered sagittal-plane control under high fatigue.

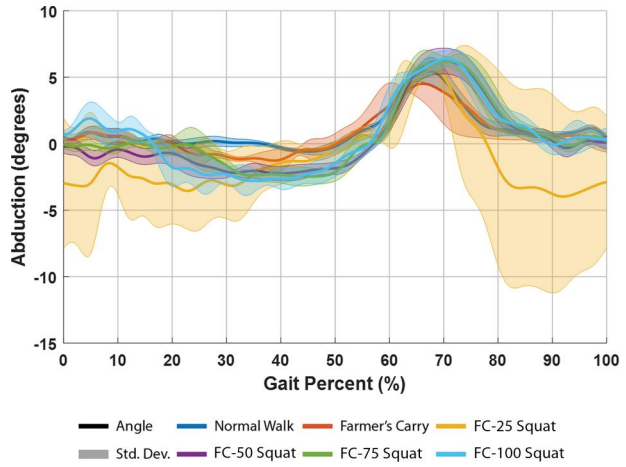

Fig. 6 Abduction angle mean and standard deviation versus percent gait: Abduction waveforms (positive = abduction) show near-neutral values at initial contact, a small early-stance valley (∼–2.5 deg), and a late-swing peak around ∼5 deg across all conditions. Variability concentrates in late swing (≈70–85% gait) and is largest for FC and FC-25, consistent with a transient frontal-plane destabilization during load-only and early-fatigue trials. Overall waveform shape and amplitude are preserved across fatigue levels.

The most prominent change occurred in late swing (≈60–80%), where abduction peaked at ∼5 deg across conditions which coincided with the timing of the swing-phase flexion peak. Variability was highest in this region: the farmer's-carry (FC) and FC-25 trials showed the largest standard deviations, with FC reaching a maximum variation of ∼8 deg near ∼85% of the gait cycle. Following the late-swing peak, abduction decreased through terminal swing (≈85–100%) and returned to near-initial values by the next heel strike.

3.3 Internal Rotation. Knee internal rotation displayed greater variability across the gait cycle, Fig. 7, compared to flexion and abduction. During the initial 0–30% of the gait cycle, internal rotation values began in close proximity across all conditions, generally between –15 deg and –25 deg, but no consistent ordering

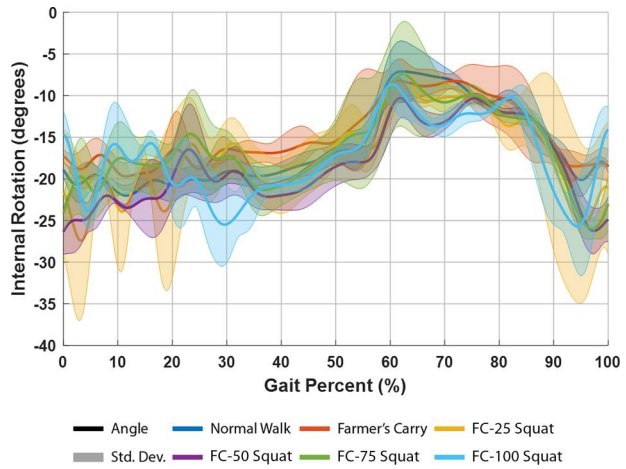

Fig. 7 Internal rotation angle mean and standard deviation versus percent gait: Internal rotation profiles begin clustered (≈ –20 deg to –25 deg), converge during midstance, peak near ∼60% gait, and then drop sharply before terminal contact. Variability is greatest early (0–30%) and late (80–95%) in the gait cycle and is highest in the early-fatigue condition (FC-25), suggesting transient transverse-plane destabilization prior to midfatigue adaptation.

or pattern was observed among the trials. Between 40% and 55%, all conditions converged into a narrower range of values. Following this convergence, internal rotation increased steadily and reached a peak near 60% gait across all trials. After this peak, internal rotation decreased gradually until approximately 80% of the gait cycle. A sharp decline occurred between 80% and 95%, followed by a return to initial values just prior to heel strike.

Under NW, internal rotation began around −21 deg, increased gradually to approximately −7 deg before terminal swing, and then returned toward the initial value (∼−21 deg) by the ensuing heel strike.

Across the entire gait cycle, the internal rotation profiles shared similar overall shapes, with early fluctuations, midstance convergence, a common peak at 60%, and a sharp drop before terminal contact. Standard deviation bands were widest during the first 30% and final 15% of the gait cycle, particularly in the farmer's carry and squat trials.

3.4 Clinical Angle Mean Standard Deviation. The variability of the clinical angles across trials, measured as the standard deviation, is summarized in Fig. 8. For each trial, the standard deviation of knee flexion, abduction, and internal rotation was averaged across the gait cycle.

Flexion showed the greatest variability among the three angles. The highest values occurred in the farmer's carry (4.56 deg) and FC-100 squats (4.69 deg) conditions. The lowest variability was observed during normal walking (2.04 deg). Flexion variability generally increased with squat repetitions, with the exception of FC 50 squats, which showed a temporary decrease compared to FC-25 squats.

Abduction remained low in variability across all trials. The highest value occurred in FC-25 squats (3.51 deg), while other squat trials ranged narrowly between 0.60 deg and 0.67 deg. The farmer's carry condition showed a moderate value of 0.66 deg, and normal walking recorded the lowest at 0.41 deg.

Internal rotation showed moderate variability, with peak values in the FC-25 squats trial (4.20 deg). Values decreased in FC-50 (2.07 deg) and increased slightly in FC-75 (3.08 deg). The FC-100 squats

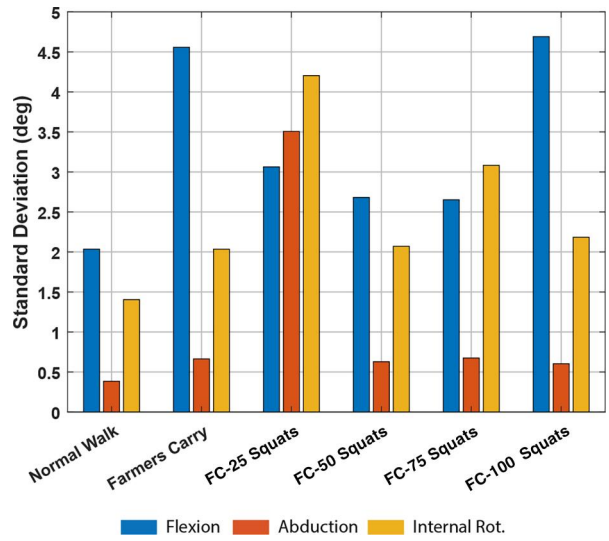

Fig. 8 Clinical angle mean standard deviation: Bar plot of the gait-cycle-averaged standard deviation (deg) for flexion, abduction, and internal rotation across conditions. Flexion shows the largest variability, lowest in NW (∼2.0 deg) and higher in FC (∼4.6 deg) and FC-100 (∼4.7 deg). Abduction variability is generally low (NW ∼0.5 deg; most trials ∼0.6–0.7 deg) but elevated in FC-25 (∼3.5 deg). Internal-rotation variability is moderate (NW ∼1.4 deg; FC ∼2.0 deg) with a peak at FC-25 (∼4.2 deg) that decreases at FC-50 (∼2.1 deg) and partially rebounds at FC-75 (∼3.1 deg), aligning with a nonlinear adaptation pattern.

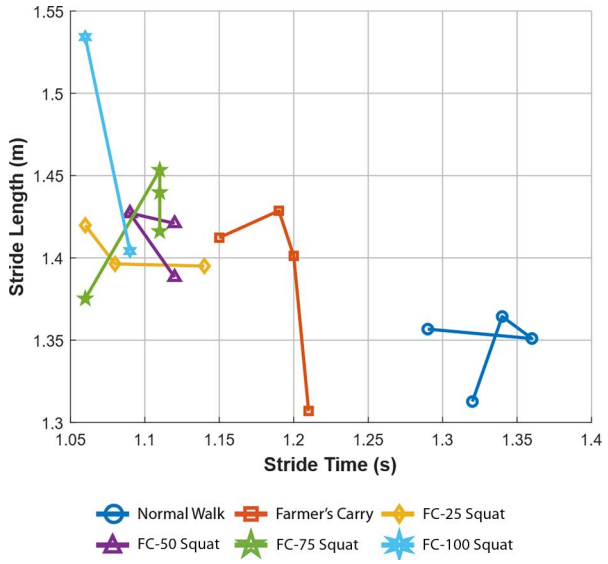

Fig. 9 Stride length versus stride time: Stride length (m) versus stride time (s) across trials. NW shows the longest stride times (≈1.30–1.36 s) with consistent lengths (∼1.31–1.36 m). FC shortens stride time (∼1.15–1.21 s) with slightly longer strides (to ∼1.42 m). Postfatigue trials (FC-25/50/75) maintain shorter stride times (∼1.06–1.14 s) with lengths ∼1.38–1.45 m. FC-100 exhibits the shortest stride times (∼1.06 s) and longest strides (to ∼1.53 m), indicating a faster, longer-step strategy under maximal fatigue and increased stride-length variability at the highest fatigue level.

trial measured 2.18 deg, while the farmer's carry and normal walking conditions measured 2.04 deg and 1.48 deg, respectively.

3.5 Stride Characteristics. Stride length and stride time for all walking trials are shown in Fig. 9. Normal walking exhibited the longest stride times, ranging from 1.28 to 1.36 s, with consistent stride lengths between 1.31 and 1.36 m. The farmer's carry condition showed reduced stride times (1.15–1.21 s) and slightly longer stride lengths (up to 1.425 m).

Postfatigue conditions demonstrated consistently lower stride times, with FC-25, 50, and 75 squats ranging from 1.05 to 1.14 s. Stride lengths in these conditions remained between 1.38 and 1.45 m. The FC-100 squats trial showed the largest variation, with stride lengths extending up to 1.53 m and the shortest stride time recorded at 1.06 s.

4 Discussion

4.1 Interaction of Fatigue and Asymmetric Loading on Knee Kinematics. This study examined how squat-induced fatigue interacts with asymmetrical loading to affect knee kinematics during walking. Across all trials, both fatigue and load altered the timing and magnitude of flexion, abduction, and internal rotation, as well as overall joint variability. These effects were most prominent in early fatigue (FC-25), diminished during midfatigue (FC-50, FC-75), and reemerged at FC-100. This pattern suggests a brief window of neuromuscular adaptation before compensatory mechanisms begin to degrade at high fatigue levels.

In contrast, a high-intensity crossover cutting study reported the opposite pattern—flexion variability increased at midfatigue (50%) and was lower during prefatigue and full-fatigue phases [3]. Additionally, an unanticipated change-of-direction study that used sprinting to induce whole-body fatigue found that fatigue and anticipation were not directly correlated, meaning that fatigue alone increases kinematic variability regardless of the task being performed [15]. These differences may be attributable to the use of whole-body fatigue protocols in those studies versus the localized fatigue protocol used in the present work.

Importantly, Kao and Lomasney's study on walking stability and kinematic variability showed that localized fatigue produces greater gait variability than whole-body fatigue [7]. This supports this study's findings: even though the exercise protocol did not involve anticipation or rapid change-of-direction factors, the localized fatigue still produced substantial increases in variability, allowing the effects of asymmetrical loading to emerge more clearly.

Flexion showed the greatest sensitivity to fatigue and asymmetrical load in this study. Peak flexion increased with squat repetitions, with the largest initial-contact and shock-absorption peaks occurring at FC-100. Event timing also shifted: swing-phase peaks were delayed, and precontact extension was incomplete at high fatigue.

The literature on fatigue-related flexion changes, however, is not consistent. Several studies report increased knee flexion after localized or distal fatigue—for example, greater loading-response flexion following plantarflexor fatigue [8] and increased heel-contact flexion after quadriceps fatigue during level walking [4]. Other work shows the opposite pattern: reduced sagittal-plane range of motion in walking after fatigue [5], or reduced initial-contact flexion (a stiffer landing strategy) during high-intensity cutting tasks [3]. Still other protocols report no significant change in walking flexion despite fatigue [6].

Taken together, prior findings indicate that fatigue can increase, decrease, or leave flexion unchanged depending on the task (walking versus cutting), the muscle group fatigued (localized versus whole-body), and the fatigue protocol used. The present study aligns most closely with the literature showing increased early-stance flexion under localized fatigue.

Abduction remained remarkably consistent in waveform and overall amplitude across all conditions, indicating that frontal-plane motion is comparatively resilient to quadriceps fatigue. This stability may reflect passive joint constraints and pelvic control strategies that preserve frontal-plane mechanics even under fatigue. However, the highest variability occurred in the left-handed farmer's-carry condition (FC), indicating that asymmetrical loading alone can introduce frontal-plane instability even when the mean abduction pattern is preserved.

This pattern partially aligns with prior unilateral load-carriage work, which reported that asymmetric loads produced no statistically significant differences in knee abduction–adduction range of motion between the loaded and unloaded limbs during walking [1]. In contrast, hip-abductor fatigue studies have shown increased knee abduction after fatigue [5], whereas the present study observed the opposite: subtle adduction shifts at specific gait events under quadriceps fatigue. A study that fatigued the quadriceps reports increased knee adduction angle (especially during swing), which supports the current study [6].

These contrasting findings highlight that the direction of abduction change depends strongly on which muscle group is fatigued and whether the perturbation arises from localized fatigue versus external asymmetrical loading.

Internal rotation exhibited greater variability than flexion or abduction, with the largest fluctuations occurring during the first 30% and final 15% of the gait cycle. Across all conditions, internal rotation profiles converged during midstance, peaked near ∼60% gait, and then declined sharply through terminal swing. Variability was greatest in the early-fatigue condition (FC-25), suggesting a brief destabilization of transverse-plane control prior to midfatigue adaptation.

The literature reports both increases and decreases in internal rotation depending on the perturbation. Increased internal rotation has been observed with added load carriage, such as weighted-vest walking [2], whereas localized quadriceps fatigue has been associated with reduced internal rotation [5]. The present study reflects elements of both findings. During the asymmetrical-load condition without fatigue (FC), internal rotation increased, consistent with the load-carriage effects reported in Ref. [2]. However, as fatigue progressed, particularly during early fatigue, internal

rotation showed reductions and altered timing consistent with quadriceps-fatigue responses described in Ref. [5]. This dual alignment indicates that internal rotation is sensitive to both external loading and localized muscular fatigue, with each perturbation shaping transverse-plane mechanics in distinct ways.

4.2 Phase-Dependent Disruptions and Compensatory Strategies. Fatigue and asymmetrical loading influenced joint behavior differently across gait phases. In early stance (heel strike to midstance), increased initial flexion and reduced extension were observed under fatigue, consistent with altered landing mechanics and diminished push-off control. During swing, terminal flexion peaks were delayed and precontact extension was incomplete in the most fatigued trials, indicating a compromised transition into stance.

A nonlinear variability pattern emerged: variability increased at FC-25, decreased during FC-50 and FC-75, and rose again at FC-100. This suggests a short-lived neuromuscular adaptation window before compensatory strategies break down. Notably, during the first loaded trial (FC), the subject adjusted to the asymmetric load without prior warm-up, functionally similar to unanticipated perturbations reported in female basketball players performing cutting tasks [15]. Their study showed that unexpected task demands and fatigue act largely independently, which aligns with our finding that asymmetric loading alone produced substantial kinematic changes even before fatigue accumulated.

The resurgence of variability at FC-100, particularly in flexion and stride measures, likely reflects failure of compensatory control. Identifying the phase and fatigue level at which variability increases sharply may help define individualized fatigue thresholds and recovery timing for repetitive or loaded tasks in rehabilitation and occupational settings.

4.3 Spatiotemporal Adjustments. In our data, stride time progressively decreased with squat repetitions, while stride length remained relatively stable through midfatigue. The shortest stride times and longest strides occurred at FC-100, suggesting a high-fatigue strategy characterized by increased cadence to maintain forward progression while unloading the fatigued limb more quickly. This compensatory pattern parallels findings from distal-muscle fatigue paradigms, where cadence increased significantly despite no change in walking velocity or overall gait pattern [8]. Such evidence supports the interpretation that cadence adjustments may serve as an early and robust mechanism for preserving walking stability under localized fatigue.

4.4 Limitations and Future Work. Although this study included only one subject, which restricts generalizability, developing subject-specific profiles is essential for understanding how fatigue and asymmetrical loading uniquely affect individual joint mechanics. Such personalized insights are critical for designing targeted rehabilitation strategies and return-to-work protocols, particularly in settings where patient-specific adaptations must be monitored over time.

Age may significantly influence neuromuscular fatigue patterns, joint stiffness, and gait adaptation strategies. Younger individuals typically demonstrate greater muscular resilience and faster recovery, while older adults often exhibit reduced strength, slower neuromuscular responses, and increased co-contraction under fatigue. Future studies should explore how age affects compensatory gait mechanisms during fatigue and asymmetrical loading to improve the relevance of findings for aging populations.

Fatigue was measured using self-reported scales rather than objective metrics such as EMG or metabolic markers. Joint moments and muscle activation patterns were not analyzed, and only the right leg was assessed, preventing insights into bilateral compensation strategies.

Future studies should incorporate larger sample sizes, bilateral kinematic and kinetic analysis, and EMG-based fatigue validation. Longitudinal studies may also help determine whether repeated exposure to asymmetric loading under fatigue leads to cumulative joint stress or altered motor patterns over time. Incorporating force plates to measure ground reaction forces would enhance understanding of kinetic asymmetries during loaded gait, offering a fuller picture of joint stress under fatigue.

5 Conclusion

This single-subject pilot examined how squat-induced fatigue interacts with asymmetrical load carriage to influence knee kinematics during walking. Fatigue altered both the magnitude and timing of key flexion events, with the largest changes emerging under high fatigue. Asymmetrical loading alone produced transient frontal-plane variability, and in combination with fatigue generated a nonlinear variability pattern—elevated at early fatigue, reduced at midfatigue, and rising again at the highest fatigue level.

Flexion was the most sensitive clinical angle, showing increased peaks and disrupted event timing with fatigue. Internal rotation exhibited greater early- and late-phase variability than abduction, while abduction remained largely consistent in shape and amplitude except for increased variability during the load-only trial. Spatiotemporally, stride time decreased as fatigue accumulated, and stride-length variability increased at maximal fatigue, suggesting a faster yet less stable strategy under the highest physiological demand.

Overall, the findings indicate that fatigue and asymmetrical loading influence knee mechanics through both independent and interacting pathways. A brief stabilization at midfatigue followed by renewed instability at high fatigue suggests a short-term adaptation window that ultimately fails. Understanding these joint-specific, phase-dependent adaptations may help inform injury-prevention strategies, rehabilitation progressions, and ergonomic guidelines for loaded walking. Larger, bilateral studies incorporating kinetics and EMG are warranted to validate and extend these observations.

Acknowledgment

The authors would like to thank the lab assistants James Cerda and Mathew Martinez for their help with data acquisition.

Funding Data

- National Science Foundation, Division of Chemical, Bioengineering, Environmental, and Transport Systems (CBET) (Grant No. 1126763; Funder ID: 10.13039/100000001).

Data Availability Statement

The datasets generated and supporting the findings of this article are obtainable from the corresponding author upon reasonable request.

References

[1] Ozgül, B., Akalan, N. E., Kuchimov, S., Uygur, F., Temelli, Y., and Polat, M. G., 2012, "Effects of Unilateral Backpack Carriage on Biomechanics of Gait in Adolescents: A Kinematic Analysis," Acta Orthop. Traumatol. Turc., **46**(4), pp. 269–274.

[2] Yang, T., Huang, Y., Zhong, G., Kong, L., Yan, Y., Lai, H., Zeng, X., Huang, W., and Zhang, Y., 2022, "6DOF Knee Kinematic Alterations Due to Increased Load Levels," Front. Bioeng. Biotechnol., **10**, p. 927459.

[3] Cortes, N., Greska, E., Ambegaonkar, J. P., Kollock, R. O., Caswell, S. V., and Onate, J. A., 2014, "Knee Kinematics Is Altered Post-Fatigue While Performing a Crossover Task," Knee Surg., Sports Traumatol., Arthrosc., **22**(9), pp. 2202–2208.

[4] Parijat, P., and Lockhart, T. E., 2008, "Effects of Quadriceps Fatigue on the Biomechanics of Gait and Slip Propensity," Gait Posture, **28**(4), pp. 568–573.

[5] Tang, Y., Li, Y., Yang, M., Zheng, X., An, B., and Zheng, J., 2022, "The Effect of Hip Abductor Fatigue on Knee Kinematics and Kinetics During Normal Gait," Front. Neurosci., **16**, p. 1003023.

[6] Murdock, G. H., and Hubley-Kozey, C. L., 2012, "Effect of a High Intensity Quadriceps Fatigue Protocol on Knee Joint Mechanics and Muscle Activation During Gait in Young Adults," Eur. J. Appl. Physiol., **112**(2), pp. 439–449.

[7] Kao, P.-C., and Lomasney, C., 2025, "Walking Stability and Kinematic Variability Following Motor Fatigue Induced by Incline Treadmill Walking," Sensors, **25**(5), p. 1489.
[8] Hunt, M. A., and Hatfield, G. L., 2017, "Ankle and Knee Biomechanics During Normal Walking Following Ankle Plantarflexor Fatigue," J. Electromyogr. Kinesiol., **35**, pp. 24–29.
[9] Grood, E. S., and Suntay, W. J., 1983, "A Joint Coordinate System for the Clinical Description of Three-Dimensional Motions: Application to the Knee," ASME J. Biomech. Eng., **105**(2), pp. 136–144.
[10] Caruntu, D. I., and Moreno, R., 2019, "Human Knee Inverse Dynamics Model of Vertical Jump Exercise," ASME J. Comput. Nonlinear Dyn., **14**(10), p. 101005.
[11] Caruntu, D. I., and Moreno, R., 2023, "Drop-Landing Inverse Dynamics Model of Human Knee," ASME J. Comput. Nonlinear Dyn., **18**(2), p. 021003.
[12] Dabirrahmani, D., Hogg, M., Smith, P. N., Bryant, A. L., and Lloyd, D. G., 2019, "Modification of the Grood and Suntay Joint Coordinate System to Improve Description of the Knee Joint Motion," J. Biomech., **88**, pp. 120–125.
[13] Caruntu, D. I., and Hefzy, M. S., 2004, "3-D Anatomically Based Dynamic Modeling of the Human Knee to Include Tibio-Femoral and Patello-Femoral Joints," ASME J. Biomech. Eng., **126**(1), pp. 44–53.
[14] Caruntu, D. I., Hefzy, M. S., Goel, V. K., Goitz, H. T., Dennis, M. J., and Agrawal, V., 2003, "Modeling the Knee Joint in Deep Flexion: Thigh and Calf Contact," Summer Bioengineering Conference, Key Biscayne, FL, June 25–29, pp. 459–460.
[15] Zhu, A., Gao, S., Huang, L., Chen, H., Zhang, Q., Sun, D., and Gu, Y., 2024, "Effects of Fatigue and Unanticipated Factors on Knee Joint Biomechanics in Female Basketball Players During Cutting," Sensors (Basel, Switzerland), **24**(14), p. 4759.